




Interlocking metasurfaces

Ophelia Bolmin¹, Benjamin Young¹, Nicholas Leathe¹, Philip J. Noell¹, and Brad L. Boyce^{1,*} 

¹ Sandia National Laboratories, Albuquerque, NM 87185, USA

Received: 15 November 2022

Accepted: 22 November 2022

Published online:

1 January 2023

This is a U.S. Government work and not under copyright protection in the US; foreign copyright protection may apply 2022

ABSTRACT

Interlocking metasurfaces (ILMs) are architected arrays of mating features that enable joining of two bodies. Complementary to traditional joining technologies such as bolts, adhesives, and welds, ILMs combine ease of assembly, removal, and reassembly with robust mechanical properties. Structural in nature, they act in a quasi-continuous manner across a surface and enable joining of complex surfaces, e.g., lattices. In this perspective, we define an ILM, begin exploring the design domain and illustrate its breath, and pragmatically evaluate mechanical performance and manufacturability. ILMs will find applications in various fields from aerospace to micro-robotics, civil engineering, and prosthetics.

Introduction

Metasurfaces have been shown to elicit remarkable properties not found in bulk counterparts in domains such as photonics and electromagnetics [1–6]. Here, we extend the concept of a metasurface to the domain structural materials, where architected ‘interlocking metasurfaces’ (ILMs, Fig. 1) imbue mechanically-robust adhesive qualities to any patternable surface. As an alternative to traditional joining technologies, such as welds, adhesives, and fasteners, ILMs enable joining of complex shapes, e.g., lattices and cellular materials (Fig. 1c). ILMs are distinct from these traditional joining technologies, as illustrated in Fig. 1.

Unlike adhesives, they are made directly from the native base material, and thus can withstand the same thermal and chemical exposure as the base material. Unlike welds, ILMs support forces across a surface rather than at a seam, and are non-permanent. And unlike bolts, they are integral to the bodies they attach, requiring no additional parts for assembly.

We define ILMs here as *an array of features across a surface that transmit force and constrain motion between adjoining bodies in one or more directions*. By this definition, there are already a few significant commercialized examples of ILMs including Velcro™, and in children’s toys such as LEGOs™. Moreover, interlocking feature arrays have been used on a few

Handling Editor: C. Barry Carter.

Address correspondence to E-mail: blboyce@sandia.gov

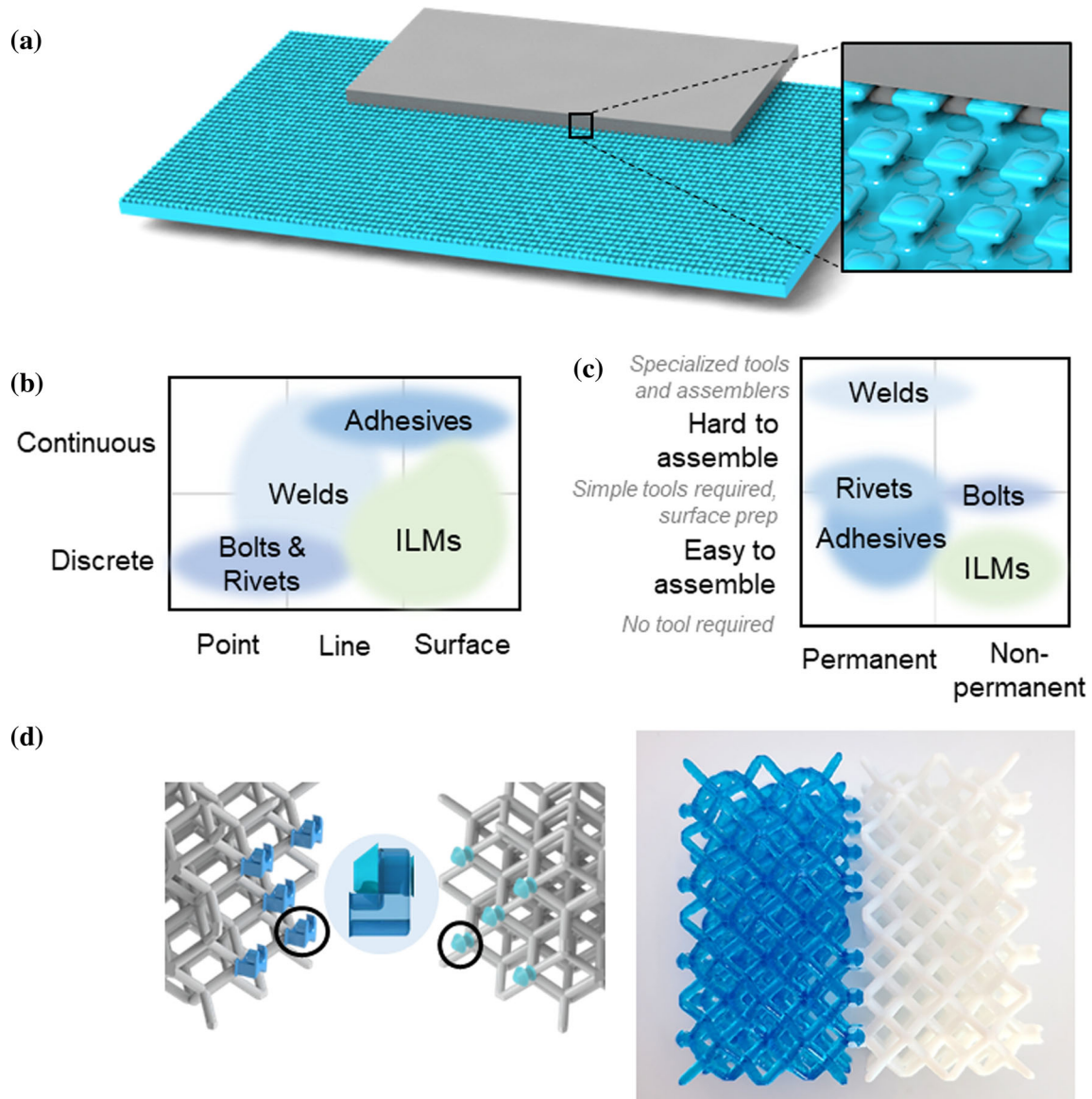


Figure 1 (a) ILMs are architected arrays of interlocking features that transmit force and restrain motion between adjoining bodies. (b) They are complementary to traditional joining technologies occasions to facilitate precise assembly in micro-fabricated parts [10–13], although usage in that field does not appear to have reached widespread adoption or commercialization. In spite of these examples, engineers have not thoroughly explored the design space of architected interlocking feature arrays. Through topological design and appropriate materials selection, it is possible to envision ILMs that can carry immense forces, with effective interfacial strengths that are a significant fraction of the base material strength (Supplemental S1), and optimized

acting in a quasi-continuous manner across a surface. (c) They form non-permanent joints that are easy to assemble, and (d) can enable joining of complex parts such as lattices.

through intentional architecting to satisfy a variety of engineering objectives.

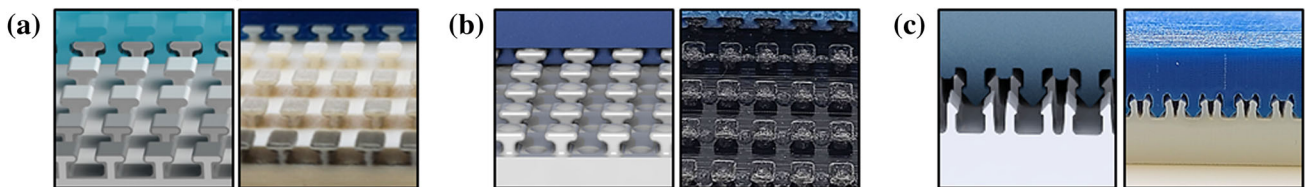
The purpose of this brief communication on ILMs is threefold: (1) illustrate a broad diversity of ILM design concepts, (2) discuss the pathways to evaluate and certify ILMs for engineering applications, and (3) discuss the role that manufacturing constraints play on ILM design.

A palette of interlocking metasurfaces

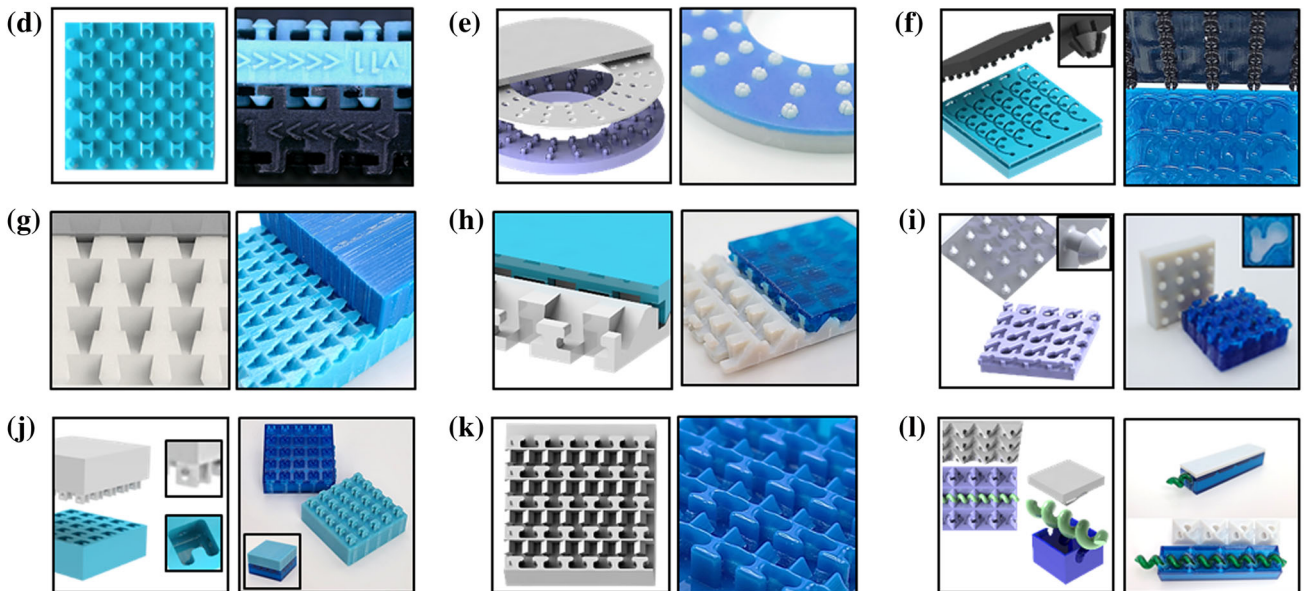
To illustrate the concept of an interlocking metasurface, fifteen demonstrator designs are shown in Fig. 2. Each concepts has unique attributes that distinguishes it from the others, illustrating the breadth of possibilities within the ILM design space. The present selection aims to demonstrate joining of planar and non-planar surfaces. In all but one case (*l*), joining occurs between two adjacent bodies with topological features inscribed into the surfaces of the

adjoining bodies. Figure 2 includes both the CAD models and physical examples printed via a polyjet additive manufacturing process (Supplemental S2). The two mating counter surfaces are modeled and printed in distinct colors in Fig. 2 to enhance visualization, though the mating counter surfaces need not be constructed from dissimilar materials. Designs *a–c*, *m*, and *o* are 2D extruded concepts. All other designs present 3D unit cell topologies. In most designs, the mating surfaces are topologically distinct on the top and bottom half (*i.e.*, male and female); however, in a

Planar surfaces; 2D unit cells



Planar surfaces; 3D unit cells



Non-planar surfaces

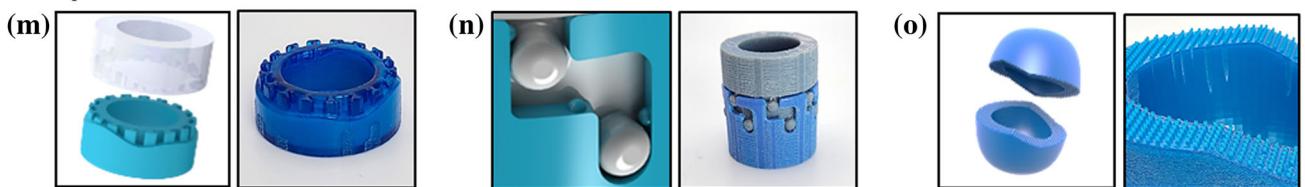


Figure 2 15 variations on an interlocking metasurface illustrate the breadth of the design space. CAD models (left panels) are shown next to physical as-manufactured ILMs (polymer jetting

technology, right panels) for each design. Each design has unique topological attributes that differentiates its function from the other examples.

few designs (*a, b, d, k*) the surfaces are identical and self-mating (*i.e.*, androgynous).

The engagement and removal trajectories, as well as the associated requisite forces, are prescribed by the unit cell topology and placement. Once engaged, the joined surfaces are maintained by mechanical interference between the mating surfaces. Designs *a–e, g–k, m* and *o* have linear engagement trajectories and are engaged via a sliding action parallel to the supporting surfaces (*a, b, d, g*), a vertical snapping action (*c, e, j, k, m, o*), or compound sliding actions (*h, i*). Designs *f* and *n* are engaged by following a curved trajectory and a combination of linear sliding and rotating actions, respectively. Design *l* exhibits a third body engaged via a linear helicoidal trajectory. Designs *d–l* and *n* create a fully locked joint by restricting all relative motions between the mating surfaces.

All designs have distinct unit cells of various complexity. Designs *a, b*, and *m* are composed of *T*-shaped interlocking features that engage through an interference fit; the engagement and removal forces are governed by dimensional tolerances and surface roughness (Fig. 2a, b, and m). Design *a* features a gradient of materials across the surface to provide distributed mechanical properties. Design *b* have hemispherical domes at the top of each *T*, and complementary conformal dimples on the counter surface to create a snapping action during engagement and removal. Design *m* has *T*-shaped features that allow joining of non-planar surfaces. Snapping features similar to design *b* are used on three mating sides of the unit cell in design *j* (Fig. 2j). Designs *c, e, f*, and *o*, are composed of arrow-like features that protrude from at least one of the joining surfaces and bend elastically to engage. The interlock is maintained by engagement of the arrow tips. Design *c* features 2D split arrows (in white in Fig. 2c) that engage with opposite full arrows and wedges; the wedges prevent the split arrows from fully returning to their undeformed state to maximize contact surfaces. Arrow and *T* features are integrated into design *k* to form a hybrid design and further constrain the assembly (Fig. 2k). Designs *e* and *f* are composed of 3D circular split arrows that engage by snapping into pin holes (Fig. 2e and f). The arrows arrangement in design *e* allows engagement at multiple angles. Design *f* is fully engaged by sliding the split arrows along a curved path after initial engagement and is locked by a second snapping action at the end of the path.

Following a similar engagement action, designs *i* and *n* feature protruding pins (in white and gray in Fig. 2i and n, respectively) that slide along a compound zig-zag path and snap to lock at the end of the path. Design *d* is composed of protruding pins and hook features that are intentionally not geometrically isometric in the plane to allow engagement in one prescribed direction only. Designs *g* and *h* are composed of interlocking dovetails that allow engagement when surfaces slide past each other at a 45 degrees angle to the vertical (Fig. 2g, h). Design *h* locks in place via a second in-plane sliding action to engage the top surface (in blue in Fig. 2h) into a snapping *T* feature (in white in Fig. 2h). Finally, design *l* is composed of conformal pyramids that restrain motion in the plane and is locked in place via insertion of a third helicoidal body (Fig. 2l).

There are many more ILM topologies to be designed. In addition to variations of the topologies showed in Fig. 2, one can imagine new designs that allow for non-planar engagement trajectories (analogous to a zipper) or that are maintained using other multi-body forces, *e.g.*, electrostatic, magnetic, capillary and Van der Waals forces. Furthermore, generative design and topological optimization tools, which are increasingly used in metamaterial design [1–4], have the potential to uncover new, non-intuitive ILM architectures.

Key performance metrics

In this section, the key structural performance metrics for ILMs are considered: engagement and removal forces, and tensile strength. In most designs, the engagement and removal forces are governed by contact properties: surface roughness, dimensional tolerances, interference fits, and snap fits. Owing to the complexity associated with accurately modeling gross sliding contact of complex mating surfaces, the evaluation focused on experimental measurements (Supplemental S1). Simple elastic finite element analysis (FEA, Supplemental S1) models were developed as a complementary characterization tool to identifying regions of stress concentration, *i.e.*, the failure points in tensile experiments.

For a given material, unit cell topology is a key factor governing ILMs mechanical properties. Figure 3 shows experimental estimates of the engagement, removal forces and tensile strength of two

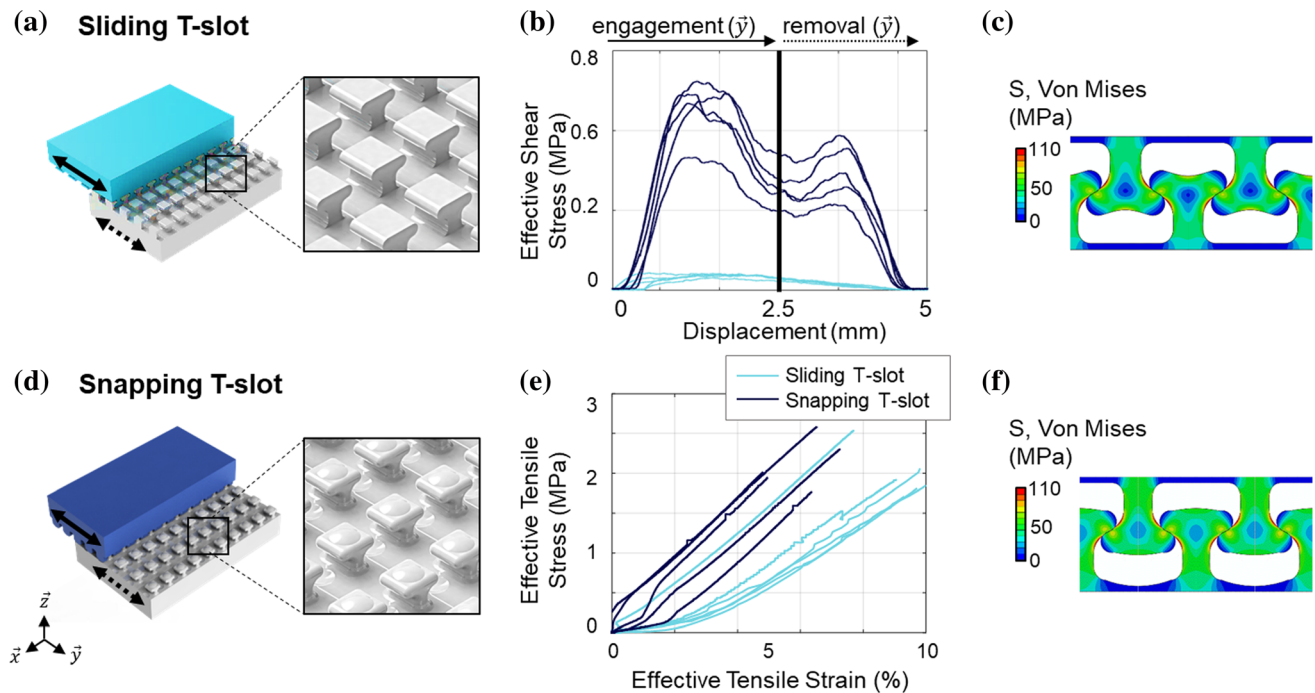


Figure 3 Two variations on *T*-slot ILMs are compared: the sliding *T*-slot design engages via dimensional tolerance interference fits (a), and the snapping *T*-slot via snapping features (d). Engagement

and removal stresses were compared in (b) and tensile response was characterized in (e). Elastic FEA simulations were used to evaluate the Von Mises stress distribution in (c) and (f).

representative interference fit-based designs. The two designs studied here were selected here for their inherent simplicity (2D extruded *T*-shaped designs), although any design could be evaluated by such methodology. The sliding *T*-slot locks in place entirely by geometric tolerance interference between the two *T*-like shapes whereas the snapping *T*-slot uses the addition of a dome-like features and complementary dimple on the mating counter surface to facilitate a snapping action. As a comparison to one another, they illustrate how modifications to unit cell topology influence mechanical properties. The stress-displacement curves (Fig. 3b) reveal that by altering the unit cell shape, the engagement forces can be dramatically altered. The sliding *T*-slot (Fig. 3a) was engaged by mechanical interference and associated sliding friction, which increased as the contact area continued to increase during engagement. In contrast, the snapping *T*-slot (Fig. 3d) was designed with a dome feature that created an extra interference-based energy barrier for engagement and removal. The snapping *T*-slot also was stiffened in out-of-plane tension, due to the presence of the reinforcing dome as confirmed experimentally (Fig. 3e) and in finite element analysis (Fig. 3c and f). Both designs

failed in a quasi-brittle manner at the locations of highest stress concentration as predicted in the finite element simulations. More details are provided in Supplemental S1, and a second example of how topology influence mechanical properties in an arrow-shaped design is detailed in Supplemental S3.

Manufacturing considerations

The examples shown in the previous sections were prototyped using commercial additive manufacturing. Additive manufacturing offers an agile approach, and with advances in this maturing technology, ILMs can be produced in a wide variety of materials (polymers, ceramics, metals) at scales ranging from micrometers to meters [5–12]. Figure 4 shows designs printed using various additive processes in different materials and at different scales (material jetting in Fig. 4a, projection micro stereolithography in Fig. 4b, multiphoton lithography in Fig. 4c, and laser powder bed fusion in Fig. 4d; see supplemental S2). However, for engineering applications that require superior material properties, or in commercial applications in large volumes, it is conceivable that ILMs could be fabricated using many

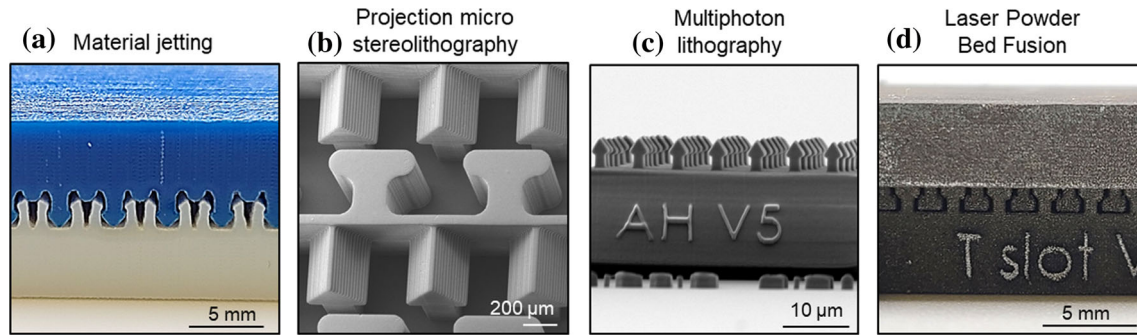


Figure 4 Examples of different ILMs at different length scales and in different materials. While these four cases involve AM techniques, ILMs are not limited to AM.

conventional manufacturing techniques ranging from injection molding [13–15] to electric discharge machining (EDM) [16–18] and lithographic micro-fabrication [19–23].

Each manufacturing technology involves process-specific design-limiting factors. The first consideration will be the native material(s) and manufacturing process(es) of the adjoining bodies. For example, an ILM patterned integrally onto the surface of a cinder block might be formed by modifying the molding/casting process, or post-forming via a subsequent grinding process. On the other hand, an ILM used to adjoin an additively manufactured steel lattice to a flat aluminum sheet might employ arrow-like insertion features on the lattice surface that insert into an array of punched holes on the sheet. Setting aside the manufacturing limitations of the adjoining bodies, there are several additional factors to consider regarding the selection of an appropriate manufacturing process: (1) geometric limitations including minimum feature size and design rules, (2) compatible materials and their associated properties in the as-manufactured state, and (3) surface condition including surface roughness and damage, (4) production time, (5) production volume, and (6) costs, including both one-time setup costs, and per-unit costs. The material selection affects ILM strength, while the achievable topologies and surface roughness influence the engagement and removal trajectories and forces. In ILM manufacturing, surface roughness is a critical, non-trivial consideration; initial and repeated engagement and removal actions lead to significant tribological changes that in turn influence the required forces (see Supplemental S4). Surface roughness induced topological variations can be mitigated by pre-conditioning parts before use, or by using solid lubricant coatings to prevent

uncontrolled wear and tear of the mating features surfaces [24, 25].

Summary, prospective applications, and open questions

The purpose of this introductory communication has been to define an ILM, provide a range of examples illustrating the breadth of the design space, and begin to explore the basic elements of performance evaluation and manufacturability. ILMs combine ease of assembly, removal, and reassembly with robust mechanical properties arising from their quasi-continuous operation over a surface and the associated distributed loading capabilities.

It is easy to envision a myriad of prospective uses for ILMs. For assembly in space, ILMs preclude the dangers of loose fasteners or the complexity of assembly tools. In micro-robotics ILMs offer integral attachment and alignment features that cannot be achieved with traditional joining. In the field of prosthetics, ILMs offer a pathway to integrate tailored patient-specific structural members without the need to introduce additional materials into the body. Beyond the single-function ILMs described herein, it is also possible to envision multifunctional ILMs such as electrical interconnects, *e.g.*, non conducting ILMs that integrate electrical conductors for information or power transmission while simultaneously providing a robust structural connection between the adjoining bodies. From these few quick examples, many more ILM applications can be explored.

The relatively unexplored domain of ILMs opens up immediate research avenues. With regard to design, ILM topologies could be designed through generative multi-objective optimization schemes, as

has previously been demonstrated for structural lattices (e.g., [26–29].), and metasurfaces (e.g., [1–4].). Going beyond the simple first-order metrics described herein, there are other critical performance metrics to investigate including how ILMs respond to shock, vibration, and fatigue, as is evaluated for conventional joining technologies [30–41], and how the surfaces degrade during repeated assembly and disassembly. With regard to materials, there is a wide range of pathways to contemplate from the compatibility of dissimilar materials in ILMs to possible surface modifications to alter the effective friction coefficient of the surfaces. Finally, the role of manufacturing defects, both internal and surface defects, on ILMs performance should be considered.

Acknowledgements

The authors thank Benjamin White and Anthony Garland for the discussions about this work. The authors thank David Saiz for printing the 316 stainless steel prints, Bryan Kaehr and Emily Huntley for printing the Nanoscribe prints, Benjamin Klitsner for laboratory support, and Boston Microfabrication for the projection multiphoton stereolithography parts. This work was performed, in part, at the Center for Integrated Nanotechnologies, an Office of Science User Facility operated for the U.S. Department of Energy. Sandia National Laboratories is a multi-mission laboratory managed and operated by National Technology and Engineering Solutions of Sandia LLC, a wholly owned subsidiary of Honeywell International Inc., for the U.S. Department of Energy's National Nuclear Security Administration under contract DE-NA0003525. The views expressed in the article do not necessarily represent the views of the U.S. Department of Energy or the United States Government.

Author contributions

OB: design concepts, simulation, original draft, editing; BY: design concepts, data acquisition, editing; NL: design concepts, application concepts; PJN: design concepts, draft editing, project leadership, BLB: design concepts, editing, project leadership.

Data and code availability

The data presented in this manuscript will be made available upon request.

Declarations

Conflict of interest The authors acknowledge the submission of a US patent application related to the concepts elucidated in Fig. 2.

Ethical approval No human tissues were involved in this study.

Supplementary Information: The online version contains supplementary material available at <http://doi.org/10.1007/s10853-022-08015-9>.

Open Access This article is licensed under a Creative Commons Attribution 4.0 International License, which permits use, sharing, adaptation, distribution and reproduction in any medium or format, as long as you give appropriate credit to the original author(s) and the source, provide a link to the Creative Commons licence, and indicate if changes were made. The images or other third party material in this article are included in the article's Creative Commons licence, unless indicated otherwise in a credit line to the material. If material is not included in the article's Creative Commons licence and your intended use is not permitted by statutory regulation or exceeds the permitted use, you will need to obtain permission directly from the copyright holder. To view a copy of this licence, visit <http://creativecommons.org/licenses/by/4.0/>.

References

- [1] Jafar-Zanjani S, Inampudi S, Mosallaei H (2018) Adaptive genetic algorithm for optical metasurfaces design. *Sci Rep* 8(1):1–16
- [2] Li D et al (2012) Design of an acoustic metamaterial lens using genetic algorithms. *J Acoust Soc Am* 132(4):2823–2833
- [3] Xu D et al (2021) Efficient design of a dielectric metasurface with transfer learning and genetic algorithm. *Opt Mater Express* 11(7):1852–1862
- [4] Zhu R et al (2020) Multiplexing the aperture of a metasurface: inverse design via deep-learning-forward genetic algorithm. *J Phys D Appl Phys* 53(45):455002

- [5] Tan LJ, Zhu W, Zhou K (2020) Recent progress on polymer materials for additive manufacturing. *Adv Funct Mater* 30:2003062
- [6] Lakhdar Y et al (2021) Additive manufacturing of advanced ceramic materials. *Prog Mater Sci* 116:100736
- [7] Lewandowski JJ, Seifi M (2016) Metal additive manufacturing: a review of mechanical properties (postprint). *Annu Rev Mater Res* 46:151–186
- [8] Goh GD et al (2019) Recent progress in additive manufacturing of fiber reinforced polymer composite. *Adv Mater Technol* 4(1):1800271
- [9] Parandoush P, Lin D (2017) A review on additive manufacturing of polymer-fiber composites. *Compos Struct* 182:36–53
- [10] Boutin C, Schwan L, Dietz M (2015) Elastodynamic meta-surface: depolarization of mechanical waves and time effects. *J Appl Phys* 117:064902
- [11] Esteve F et al (2017) Micro-additive manufacturing technology. *Micro-manufacturing technologies and their applications*. Springer, pp 67–95
- [12] Greer C et al (2019) Introduction to the design rules for metal big area additive manufacturing. *Addit Manuf* 27:159–166
- [13] Bonenberger PR (2005) Enhancements. In: Bonenberger PR (ed) *The first snap-fit handbook*, 2nd edn. Hanser, Cincinnati, pp 95–134
- [14] Chen Z, Turng LS (2005) A review of current developments in process and quality control for injection molding. *Adv Polym Technol J Polym Process Inst* 24(3):165–182
- [15] German RM (2013) Progress in titanium metal powder injection molding. *Materials* 6(8):3641–3662
- [16] Mohd Abbas N, Solomon DG, FuadBahari M (2007) A review on current research trends in electrical discharge machining (EDM). *Int J Mach Tools Manuf* 47(7):1214–1228
- [17] Yi SM et al (2008) Fabrication of a stainless steel shadow mask using batch mode micro-EDM. *Microsyst Technol* 14(3):411–417
- [18] Ho KH, Newman ST (2003) State of the art electrical discharge machining (EDM). *Int J Mach Tools Manuf* 43(13):1287–1300
- [19] Reed ML, Han H, Weiss LE (1992) *Silicon micro-velcro*. Wiley Online Library
- [20] Prasad R, Bohringer KF, MacDonald NC (1995) Design, fabrication, and characterization of single crystal silicon latching snap fasteners for micro assembly, Cornell University
- [21] Gillies AG, Fearing R (2010) A micromolded connector for reconfigurable millirobots. *J Micromech Microeng* 20(10):105011
- [22] Ko H et al (2009) Hybrid core– shell nanowire forests as self-selective chemical connectors. *Nano Lett* 9(5):2054–2058
- [23] Brown JJ, Bright VM (2016) Mechanical interfacing using suspended ultrathin films from ALD. *J Microelectromech Syst* 25(2):356–361
- [24] Donnet C, Erdemir A (2004) Solid lubricant coatings: recent developments and future trends. *Tribol Lett* 17(3):389–397
- [25] Scharf T, Prasad S (2013) Solid lubricants: a review. *J Mater Sci* 48(2):511–531
- [26] Parker B, Singh HK, Ray T (2021) Multi-objective optimization across multiple concepts: a case study on lattice structure design. In: *Genetic and evolutionary computation conference*, Lille, France
- [27] Abdeljaber O, Avci O, Inman DJ (2016) Optimization of chiral lattice based metastructures for broadband vibration suppression using genetic algorithms. *J Sound Vib* 369:50–62
- [28] Xu W, Wang W, Yang T (2013) Multi-objective optimization of layered elastic metamaterials with multiphase microstructures. *J Vib Acoust* 135(4):041010
- [29] Garland AP et al (2021) Pragmatic generative optimization of novel structural lattice metamaterials with machine learning. *Mater Des* 203:109632
- [30] Patterson E (1990) A comparative study of methods for estimating bolt fatigue limits. *Fatigue Fract Eng Mater Struct* 13(1):59–81
- [31] Yang L et al (2021) Analysis of competitive failure life of bolt loosening and fatigue. *Eng Fail Anal* 129:105697
- [32] Pascoe JA, Alderliesten RC, Benedictus R (2013) Methods for the prediction of fatigue delamination growth in composites and adhesive bonds – a critical review. *Eng Fract Mech* 112–113:72–96
- [33] Jin H et al (2011) Fracture and fatigue response of a self-healing epoxy adhesive. *Polymer* 52(7):1628–1634
- [34] Zuo P, Vassilopoulos AP (2021) Review of fatigue of bulk structural adhesives and thick adhesive joints. *Int Mater Rev* 66(5):313–338
- [35] Lawrence F, Ho N, Mazumdar PK (1981) Predicting the fatigue resistance of welds. *Annu Rev Mater Sci* 11(1):401–425
- [36] Radaj D, Sonsino C, Fricke W (2009) Recent developments in local concepts of fatigue assessment of welded joints. *Int J Fatigue* 31(1):2–11
- [37] Zadoks R, Yu X (1997) An investigation of the self-loosening behavior of bolts under transverse vibration. *J Sound Vib* 208(2):189–209
- [38] Gao D, Yao W, Wu T (2019) Failure analysis on the axial-connected bolts of the thin-walled cylinder under random vibration loading. *Eng Fail Anal* 105:756–765

- [39] Zaki AM, Nassar SA, Yang X (2010) Vibration loosening model for preloaded countersunk-head bolts, pp 361–371
- [40] Guyott C, Cawley P (1988) The ultrasonic vibration characteristics of adhesive joints. *J Acoust Soc Am* 83(2):632–640
- [41] Du Y, Shi L (2014) Effect of vibration fatigue on modal properties of single lap adhesive joints. *Int J Adhes Adhes* 53:72–79

Publisher's Note Springer Nature remains neutral with regard to jurisdictional claims in published maps and institutional affiliations.